

Gravitational Wave Polarization Analysis of GW170814

Robert C. Hilborn^{a)}

*American Association of Physics Teachers
College Park, MD 20740*

31 January 2018

We use the results of the GW170814 gravitational wave detection by the three LIGO-VIRGO observatories to study the polarization properties of the gravitational waves. We find that there is an apparent inconsistency among the reported *pre-merger* signal amplitudes at the three detectors, the reported sky location of the source, and the linear GR model of gravitational wave polarization. The standard linear GR model accounts for the observed amplitude ratios among the three detectors only if the sky location is (just) outside the reported LIGO-VIRGO 90% confidence region and only for a limited range of orbital inclination and polarization orientation angles. Surprisingly, we find that a vector polarization model can also account for the observed amplitude ratios for that same sky location.

rhilborn@aapt.org

I. INTRODUCTION

The observation of the gravitational wave (GW) burst GW170814 by the three LIGO-VIRGO observatories¹ allows for a reasonably precise determination of the GW source location. More importantly, those observations also allow us to test predictions for the polarization modes of the GWs, something not previously possible with the prior GW observations involving just the two LIGO observatories.² General relativity (GR) predicts that the GWs will exhibit only tensor polarization modes, an aspect of GR that has not been directly tested before. The comparisons with GR predictions need to take into account the interplay among the GW source location (or equivalently, the GW wave propagation direction), the amplitudes and phases of the signals at the three observatories, the wave-front arrival times at the observatories, and the polarization properties of the GWs. The amplitudes and phase shifts depend, of course, on the orientation of the observatories' interferometer arms relative to the GW propagation direction and the GW polarization orientation.

Here we analyze the GW170814 binary black hole gravitational wave observations recorded at the Hanford, Livingston, and VIRGO gravitational wave observatories¹ in terms of the GW polarization orientation angle and the binary orbital angle of inclination. It turns out to be important to consider the full range of those angles.³ The binary black hole GW signals can be described in terms of three

phases: (1) pre-merger inspiral, (2) merger, and (3) ring-down. We will focus on using the *pre-merger* data to analyze the results because linear GR provides explicit expressions (see Section III) for the orbital angle of inclination and polarization orientation angle dependence of the signals. Numerical GR is needed to analyze the merger and ring-down modes. Using previously published results (see, for example, Ref. [4]), we will show how to use both the standard GR tensor polarization modes and “non-standard” vector polarization modes that emerge from more general metric theories of gravity,⁵⁻⁷ from vector theories of gravity,⁸ and from electromagnetism-like (E&M-like) models of gravitational waves^{9,10} to predict the ratios of the GW pre-merger amplitudes seen at the three observatories. (We will not treat the “breathing” and longitudinal polarization modes here.) By focusing on the relative amplitudes among the three observatories, we eliminate the need to take into account the evolving GW amplitude and frequency during the pre-merger inspiral.

Assuming that the GW source is a binary black hole inspiral (for which there is considerable evidence), we find an apparent inconsistency among the reported pre-merger signal amplitudes at the three observatories, the sky location of the source, and the linear GR model of the wave polarization. The vector polarization model also fails to account for the observed amplitude ratios for that sky location.

The sky location of the GW source can be determined from the arrival-time delays of the gravitational wave-front at the three observatories. However, the observed delay times may be affected by phase shifts between the detectors' responses to the polarization modes, which shifts are in general different for the different observatories and are not known a priori.¹¹ In turn, inferences about the polarization of the gravitational waves depends on the source location. We explore a range of sky locations to see if any can remove the inconsistencies, and we examine the phase shifts that occur for those conditions.

The complex interplay among the GW wave and detector parameters and the observations ought to encourage us to undertake a detailed full-parameter fit, taking into account priors of the various parameters and their measurement error distributions and appropriate weighting factors. For the sake of laying out the physics underlying the analysis, we will take a simplified approach that delivers a consistent set of results, leaving the more detailed analysis for latter work.

II. GRAVITATIONAL WAVE AND DETECTOR GEOMETRY

The amplitude and phase of the binary black hole GW signals observed at the LIGO-VIRGO observatories depend on the binary orbit's angle of inclination relative to the direction from the source to the observation point and on the orientation of the GW polarization directions relative to the interferometer arms of the GW detectors. We will use this section to introduce unit vectors that specify the geometry.

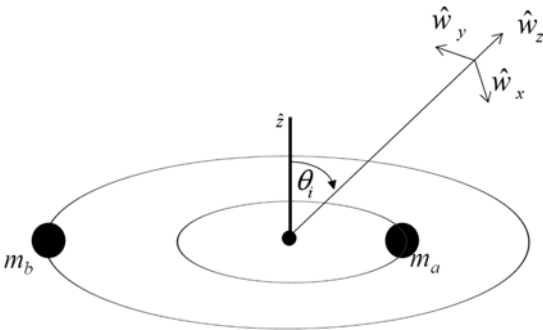


FIG. 1. A perspective view of the orbits for two orbiting masses m_a and m_b , showing the definition of the angle of inclination θ_i and the gravitational wave unit vectors. The unit vector \hat{z} is perpendicular to the plane of the orbit. The gravitational wave unit vector \hat{w}_z points from the center of mass to the observation point. \hat{w}_x lies in the \hat{z} - \hat{w}_z plane. \hat{w}_y is perpendicular to that plane.

Figure 1 shows the standard definition of the binary orbit's angle of inclination θ_i between \hat{w}_z , pointing from the source to the observation point, and \hat{z} normal to the orbital plane. The unit vector \hat{w}_x lies in the \hat{z} - \hat{w}_z plane while \hat{w}_y is perpendicular to that plane.

In this paper, we will focus on the Hanford (H), Livingston (L), and VIRGO (V) observatories of the LIGO-VIRGO collaboration. Figure 2 indicates the standard way of specifying the detector arms' orientation in terms of the unit vectors \hat{d}_x and \hat{d}_y .

The local vertical direction is along \hat{d}_z . The geometry of the GW observatories is given by the latitude and longitude of the vertex of the interferometer arms and unit vectors giving the orientation of the two interferometer arms in a plane perpendicular to the local vertical. In the GW literature, the angle of the x -arm of the interferometer is often indicated by α_D , measured counterclockwise from local true North or, less often, by the angle ψ_D relative to the line of nodes.

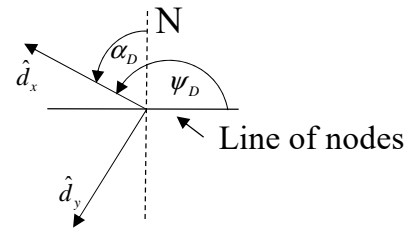


FIG. 2. The definition of the gravitational wave detector interferometer orientation angles α_D and ψ_D , (where $D = H, L, \text{ or } V$). The local vertical \hat{d}_z (not shown) is up and out of the page. \hat{d}_x and \hat{d}_y define the detector plane. The dashed line lies in the local meridian plane defined by \hat{d}_z and the line connecting Earth's two poles. The solid horizontal line, the "line of nodes," is the intersection between the detector plane and Earth's equatorial plane. Angles are measured counterclockwise as shown in the figure.

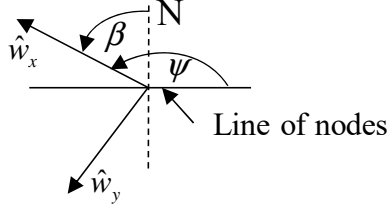


FIG. 3. The definition of the gravitational wave polarization orientation angles β and ψ . \hat{w}_z (not shown) points up out of the page. The dashed line lies in the \hat{z}_E - \hat{w}_z plane, where \hat{z}_E points from South to North on Earth. The line of nodes is the intersection of the wave front (\hat{w}_x - \hat{w}_y) plane and Earth's equatorial plane.

To calculate the GW detector signal, we also need to know the direction of propagation of the GW and the orientation of the GW polarization vectors. The propagation direction vector that passes through the center of Earth first hits Earth's surface at a point whose location we will specify in terms of latitude and longitude. In what follows, we will discuss the standard method used to find the latitude and longitude of that point for a short GW burst. However, we do not know either the angle of inclination θ_i or the polarization orientation angle. In the GW literature, the orientation of the \hat{z} - \hat{w}_z plane is sometimes specified by the angle β relative to the local true North direction at the detector location or by the angle ψ relative to the line of nodes, which is defined by the intersection of the wave front (\hat{w}_x - \hat{w}_y) plane with Earth's equatorial plane. In what follows, we will use the latter definition.

Given the information on the orientation of the GW detectors and the GW wave propagation direction and the polarization orientation, calculating the effects of the gravitational wave polarization for the LIGO-VIRGO detectors is a straightforward matter of geometry.

III. ANTENNA PATTERNS

In this section we review how to use the unit vectors introduced in the previous section to find the GW detectors' responses to GWs. We will first give the tensor polarization properties associated with the standard linear form of GR. We then show how those results are modified if we use a GW vector polarization model.

Tensor Polarization

In GR's treatment of gravitational waves,^{12,13} there are two "tensor" polarization modes, named

"plus" (+) and "cross" (\times) with amplitudes A_+ and A_\times . Far from a binary orbit GW source, the response of an interferometer-type detector to GWs is given by^{3,4,14-17}

$$\begin{aligned} A_+ &= \frac{a_{GR}(t)}{2} (1 + \cos^2 \theta_i) F_+(\hat{w}, \hat{d}) \\ A_\times &= a_{GR}(t) \cos \theta_i F_\times(\hat{w}, \hat{d}), \end{aligned} \quad (1)$$

where $a_{GR}(t)$ is an overall amplitude factor, which depends on the distance from the source to the observation point and the source properties such as orbital frequency and mass separation, which change in time during the inspiral. The response functions (antenna patterns) are

$$\begin{aligned} F_+(\hat{w}, \hat{d}) &= \frac{1}{2} \left[(\hat{w}_x \cdot \hat{d}_x)^2 - (\hat{w}_x \cdot \hat{d}_y)^2 - (\hat{w}_y \cdot \hat{d}_x)^2 + (\hat{w}_y \cdot \hat{d}_y)^2 \right] \\ F_\times(\hat{w}, \hat{d}) &= (\hat{w}_x \cdot \hat{d}_x)(\hat{w}_y \cdot \hat{d}_y) - (\hat{w}_x \cdot \hat{d}_y)(\hat{w}_y \cdot \hat{d}_x). \end{aligned} \quad (2)$$

For a periodic GW source, there is a 90° temporal phase difference between the two polarization modes.

We now express orbiting binaries' GW signal amplitude and its phase in terms of the inclination angle θ_i and the polarization angle ψ . First, to simplify notation, we define

$$\begin{aligned} f_\times(\theta_i) &= (1 + \cos^2 \theta_i) / 2 \\ f_+(\theta_i) &= \cos \theta_i \end{aligned} \quad (3)$$

and write

$$\begin{aligned} A_{\times,D}(\theta_i, \psi, t) &= a_{GR}(t) f_\times(\theta_i) F_\times(\hat{w}, \hat{d}) \\ A_{+,D}(\theta_i, \psi, t) &= a_{GR}(t) f_+(\theta_i) F_+(\hat{w}, \hat{d}), \end{aligned} \quad (4)$$

where $D = H, L, \text{ or } V$ and $\hat{d} = \hat{H}, \hat{L}, \text{ or } \hat{V}$ for the three observatories. For orbiting binaries, the pre-merger signal is approximately sinusoidal with a frequency and amplitude, both of which increase as the system radiates away GW energy and the two orbiting objects approach each other. Thus, for periods of time sufficiently short compared to the binary inspiral time, we may write the tensor signal as

$$h_{TD}(t) = A_{TD}(\theta_i, \psi, t) \cos(2\omega t + \Phi_{TD}), \quad (5)$$

where the amplitude is given by

$$A_{TD}(\theta_i, \psi, t) = \sqrt{A_{xD}^2 + A_{+D}^2} \quad (6)$$

and the phase satisfies

$$\Phi_{TD} = \cos^{-1}(A_{+D} / A_{TD}). \quad (7)$$

We will be interested in looking at ratios of amplitudes for the different observatories, for example A_{TV} / A_{TL} , and phase differences for the different observatories, for example $\Phi_{TV} - \Phi_{TL}$, as functions of the angles θ_i and ψ . As mentioned previously, using those ratios removes the effects of the time-varying frequency and amplitude during the pre-merger inspiral. Comparison with the GW170814 observations will then in principle give us information about possible values of θ_i and ψ consistent with those observations.

Vector Models

In generalized metric theories of gravity,⁵⁻⁷ GWs may have a mix of tensor and vector polarization modes. In vector theories of gravity,⁸ and in an E&M-like (vector) model of GWs,^{9, 10} the GW wave has vector polarization components (exactly like the description of polarization for E&M waves). For a simply periodic wave source, the two polarization modes have a temporal phase difference of 90° .

The two vector (v) polarization components, labeled x and y , give GW detector signal amplitudes described by

$$\begin{aligned} A_x &= a_v(t) f_x(\theta_i) F_x(\hat{w}, \hat{d}) \\ A_y &= a_v(t) f_y(\theta_i) F_y(\hat{w}, \hat{d}) \end{aligned} \quad (8)$$

where $a_v(t)$ is an overall amplitude factor and the response functions are¹⁴

$$\begin{aligned} F_x(\hat{w}, \hat{d}) &= (\vec{w}_z \cdot \vec{d}_x) (\vec{d}_x \cdot \vec{w}_x) - (\vec{w}_z \cdot \vec{d}_y) (\vec{d}_y \cdot \vec{w}_x) \\ F_y(\hat{w}, \hat{d}) &= (\vec{w}_z \cdot \vec{d}_y) (\vec{d}_y \cdot \vec{w}_y) - (\vec{w}_z \cdot \vec{d}_x) (\vec{d}_x \cdot \vec{w}_y). \end{aligned} \quad (9)$$

In an E&M-like model,^{9,10} the pre-merger dependences on the angle of inclination for a binary orbit GW source are

$$\begin{aligned} f_x(\theta_i) &= \sin 2\theta_i \\ f_y(\theta_i) &= -2 \sin \theta_i. \end{aligned} \quad (10)$$

In analogy with the linear GR model, we now express the amplitude of the vector GW signal from orbiting binaries and its phase in terms of the inclination angle θ_i and the polarization angle ψ . We define two polarization mode amplitude functions for the vector model:

$$\begin{aligned} A_{xD}(\theta_i, \psi, t) &= a_v(t) f_x(\theta_i) F_x(\hat{w}, \hat{d}) \\ A_{yD}(\theta_i, \psi, t) &= a_v(t) f_y(\theta_i) F_y(\hat{w}, \hat{d}), \end{aligned} \quad (11)$$

where again $D = H, L, \text{ or } V$ for the three observatories. For periods of time short compared to the binary inspiral time, we may write the signal as

$$h_{vD}(t) = A_{vD}(\theta_i, \psi, t) \cos(2\omega t + \Phi_{vD}), \quad (12)$$

where the amplitude is given by

$$A_{vD}(\theta_i, \psi) = \sqrt{A_{xD}^2 + A_{yD}^2} \quad (13)$$

and the phase satisfies

$$\Phi_{vD} = \cos^{-1}(A_{xD} / A_{vD}). \quad (14)$$

In parallel with the treatment of the tensor polarization model, we will be interested in looking at ratios of amplitudes for the different observatories, for example A_{vV} / A_{vL} , and phase differences for the different observatories, for example $\Phi_{vV} - \Phi_{vL}$, as functions of the angles θ_i and ψ . Comparison with the GW170814 observations will then in principle give us information about possible values of θ_i and ψ consistent with those observations.

It is important to note that the results in Eqs. (2) and (9) will hold for any gravitational wave theory since they are purely geometric expressions of what we mean by tensor polarization and vector polarization, respectively.

To calculate the various scalar products in Eqs. (2) and (9), it is helpful to express each of the vectors in terms of an Earth-fixed coordinate system with \vec{z}_E running from the South pole towards the North pole, \vec{x}_E running from the center of Earth along the prime meridian (which intersects the surface at 0° longitude) and \vec{y}_E forming a right-handed Cartesian coordinate system with \vec{x}_E and \vec{z}_E . The components of each of the detector unit vectors in the Earth-fixed system are available from the LIGO-VIRGO collaboration.^{17,18} The gravitational wave unit vectors can be expressed in terms of the Earth-fixed

unit vectors by using the source latitude and longitude and the unknown polarization orientation angle ψ .

IV. GW SOURCE LOCATION

In this section we show how to use the observed wave-front arrival-time delays among the three observatories to determine the celestial coordinates of the gravitational wave source. We assume that the GW signal duration is short (in practice from a few tenths of a second to a few seconds for recent observations) so the source location relative to the rotating and orbiting Earth does not change significantly during the wave observation time.

We denote the position of the Hanford observatory relative to the Livingston observatory as \vec{r}_{LH} and the analogous position of VIRGO as \vec{r}_{LV} . Those position vectors can be easily calculated from $(\hat{H}_z - \hat{L}_z)R_E$ and $(\hat{V}_z - \hat{L}_z)R_E$, where R_E is the radius of Earth (6.37×10^3 km), ignoring the small non-sphericity of Earth. As mentioned previously, the calculation is simplified by using components relative to the Earth-fixed frame of reference.

Given those vectors, it is easy to see that the arrival time delays are given by

$$\Delta t_{LH} = \hat{w}_z(\theta_{lat}, \phi_{long}) \cdot \vec{r}_{LH} / c \quad (15)$$

$$\Delta t_{LV} = \hat{w}_z(\theta_{lat}, \phi_{long}) \cdot \vec{r}_{LV} / c, \quad (16)$$

where θ_{lat} and ϕ_{long} are the latitude and longitude of the GW source. (Strictly speaking, those angles are the latitude and longitude of the point on Earth's surface at which the source is directly overhead at the time of the GW event.) In detail, the GW propagation unit vector can be expressed as

$$\begin{aligned} \hat{w}_z(\theta_{lat}, \phi_{long}) = & -(\cos \theta_{lat} \cos \phi_{long}) \hat{x}_E \\ & + (\cos \theta_{lat} \sin \phi_{long}) \hat{y}_E - \sin \theta_{lat} \hat{z}_E \end{aligned} \quad (17)$$

The gravitational wave speed is assumed to be the usual speed of light. Eqs. (15) and (16) provide two equations for the two unknown angles θ_{lat} and ϕ_{long} .

We will now employ the expressions derived above to extract information about the GW source location based on the observations of GW170814 described in Ref. [1]. Using the reported¹ gravitational wave-front arrival time delays, $\Delta t_{LH} = 8$ ms and $\Delta t_{LV} = 14$ ms, for Livingston-Hanford and Livingston-VIRGO respectively, and the relative position vectors \vec{r}_{LH} and \vec{r}_{LV} , we may employ Eqs. (15) and (16) to calculate the source

latitude and longitude at the time of the observations. We find for the source latitude and longitude

$$\begin{aligned} \theta_{lat} &= -49.7^\circ \\ \phi_{long} &= 77^\circ \text{ W}. \end{aligned} \quad (18)$$

The GW170814 Fact Sheet¹⁹ claims that a full GR parameter analysis yields $\theta_{lat} = -44^\circ 57^m$ and $\phi_{long} = 73^\circ \text{ W}$ for the source. Note that the results in Eq. (18) lie outside the ‘‘rapid localization’’ region described in Ref. [1] and illustrated in Fig. 4. (See Ref. [11] for a discussion of how source localization can be improved by taking into account GW polarization and assumptions about the astrophysical distribution of sources.)

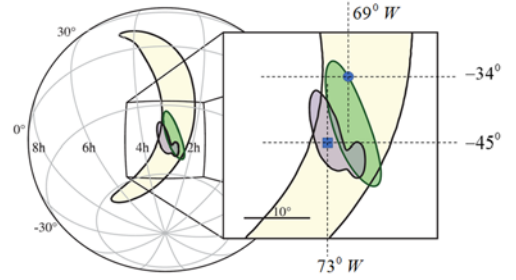


FIG. 4. Based on Fig. 3 of Ref. [1], this figure shows the location of the GW170814 source in equatorial (celestial) coordinates. The inset is a gnomonic projection. The contours represent the 90% credible regions. The light (yellow) shading is the localization using only the two LIGO sites. The intermediate (green) shading is the rapid localization results using data from all three observatories, while the darker shading (purple) is the full Bayesian localization. The filled square indicates the source location determined by LIGO-VIRGO. The small filled circle in the inset indicates the ‘‘alternative’’ source location at -34° declination and longitude 69° W discussed later in this paper. The longitudinal lines are those for the source at the time of the GW170814 event.

Figure 3 of Ref. [1] indicates that the longitude uncertainty is about $\pm 5^\circ$ (90% credibility limits) while the latitude uncertainty is about $\pm 10^\circ$. Those uncertainties are consistent with an uncertainty range based on an arrival-time uncertainty about ± 1 ms. Within those uncertainties, the latitude and longitude results found here (Eq. (18)) agree with the LIGO-VIRGO results.

To demonstrate the effect of arrival time uncertainty on the GW latitude and longitude angles, let's set $\Delta t_{LH} = 8.9$ ms and $\Delta t_{LV} = 14$ ms, for which we find $\theta_{lat} = -34^\circ$ and $\phi_{long} = 69^\circ \text{ W}$. We will return to these values later in our discussion of the

ratio of amplitudes at the various GW detectors. As indicated in Fig. 4, this location is just outside the 90% confidence range shown in Fig. 3 of Ref. [1]. The main point of this section is that the GW source location parameters are sensitive to the arrival-time delays among the three observatories. In what follows, we will initially use the LIGO-VIRGO GW170814 source location parameters.

V. POLARIZATION, ORBITAL INCLINATION AND RELATIVE AMPLITUDES

Given the source location, we now determine what limits (if any) can be placed on the orbital angle of inclination θ_i and the polarization orientation angle ψ . We will look at the predicted GW amplitude ratios (Hanford/Livingston and VIRGO/Livingston) and the corresponding signal phase differences as a function of those angles and see what ranges are consistent with the observations.

There are several complications in this analysis. First, the expressions Eqs. (1), (2), (8), and (9) come from the linear version of GR or the E&M-like model, both of which are restricted to the pre-merger GW signals emitted before the two black holes coalesce. We might expect that the polarization properties of the GWs change during the merger and ring-down phases due to the strong space-time curvature produced during those events.²⁰

In fact, we do see from the signals plotted in Fig. 1 of Ref. [1] (hereafter denoted as GW170814-Fig. 1) that the amplitude ratios change in going from the pre-merger inspiral to the merger and ring-down stages. An approximate method of handling the polarization during the early stages of the merger is given in Ref. [21]. Here we will restrict ourselves to the pre-merger phase.

The second complication comes from possible spin-orbit and spin-spin effects if the black holes are rotating. These effects will cause the orbital angular momentum direction (which is of course perpendicular to the plane of the binary orbits) to precess about the total angular momentum direction. This precession implies that the orbital angle of inclination will be modulated as a function of time, leading to a modulation in the ratio of the polarization mode amplitudes and consequently of the signal amplitudes at the detectors. Furthermore, the total angular momentum of the binary system will change because the GWs themselves carry away angular momentum. For simplicity's sake we will ignore those complications in this analysis. An analysis of GWs emitted by binary black holes with spin is given in Ref. [22].

As mentioned previously, we will examine both the standard GR prediction for GW tensor

polarization modes and a vector polarization model starting with the LIGO-VIRGO GW170814 angles for the GW wave: $\theta_{lat} = -45^\circ$ and $\phi_{long} = 73^\circ$. Later we will explore how the results vary when the source location changes.

Tensor (linear GR) polarization model

First let's look at the GR (tensor) prediction for the Livingston observatory signal as a function of the orbital angle of inclination and the polarization orientation angle, assuming the LIGO-VIRGO latitude and longitude values for the wave propagation direction. This analysis will help build our intuition about what to expect for the ratios of amplitudes among the various observatories.

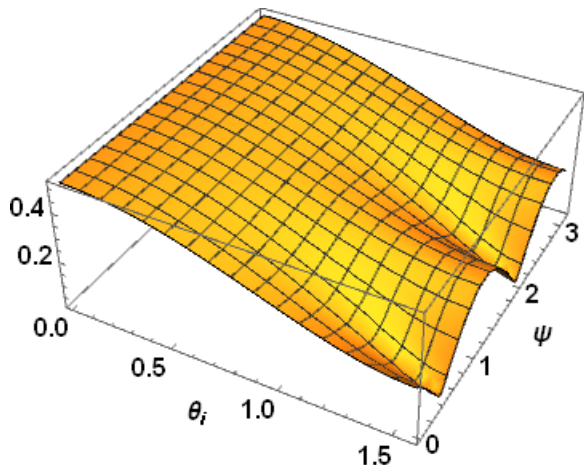


FIG. 5. The linear GR prediction for the Livingston observatory strain signal amplitude (arbitrary units) as a function of the orbital angle of inclination θ_i and the polarization angle of orientation ψ , both in radians.

For small angles of inclination (that is, the observation direction is nearly perpendicular to the plane of the binary orbit), linear GR theory (see Eq. (1)) predicts equal amplitudes for the cross and plus polarization modes. Since the temporal phase difference between the modes is $\pi/2$, we have the equivalent of “circular polarization,” for which the amplitude is independent of the polarization angle ψ as illustrated in Fig. 5.

As θ_i approaches $\pi/2$, the amplitude for the cross polarization goes to zero, leaving only the plus polarization. We see that the amplitude as a function of ψ has a periodicity of $\pi/2$, characteristic of the tensor modes of quadrupole radiation. (For vector polarization, the periodicity is π .) The plot for $\pi/2 \leq \theta_i \leq \pi$ is just the mirror image of the plot

shown in Fig. 5 (reflected in the $\theta_i = \pi/2$ line). The amplitude graphs for the Hanford and VIRGO signals are similar.

Tensor amplitude ratios for the three observatories

Let's now turn our attention to the amplitude ratios for the different observatories since those ratios are independent of the time-dependent frequency and amplitude of the GW, at least until we near the time at which the black hole merger begins. As mentioned previously, those ratios allow us to probe the polarization properties of the GWs, an aspect not possible to explore before the first “three-observatory” data from GW170814.

Using the LIGO-VIRGO numerical GR results (GW170814-Fig. 1) as good summaries of the raw data, we find that figure indicates that both the Hanford/Livingston (H/L) ratio and the VIRGO/Livingston (V/L) ratio are about 0.69 with an estimated uncertainty of about $\pm 20\%$ during the pre-merger inspiral. During the merger phase the H/L ratio is about 1 and the V/L ratio is about 0.8, in agreement with the GW170814 LIGO-VIRGO Fact Sheet.¹⁹ That change in the signal amplitude ratios indicates that the polarization of the GWs is changing during the merger compared to the pre-merger inspiral.

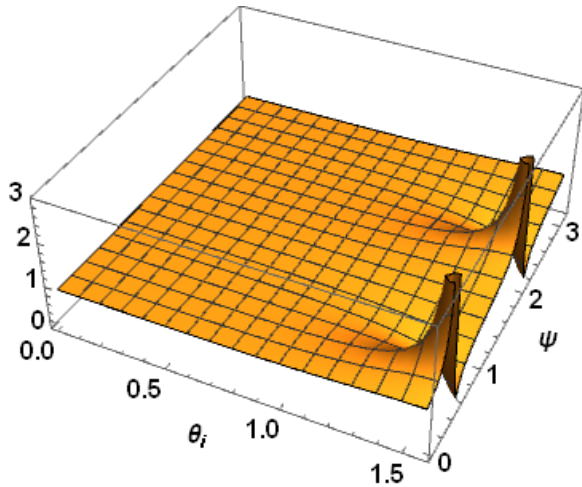


FIG. 6. The linear GR predicted ratio of the VIRGO observatory strain signal amplitude to the Livingston amplitude as a function of the orbital angle of inclination θ_i and the polarization orientation angle ψ , both in radians.

Figure 6 shows the ratio of the VIRGO amplitude to the Livingston amplitude as a function of the orbital angle of inclination and the polarization orientation angle for the linear GR model. Over most

of the angular ranges, the ratio is close to one. The large “spikes” occur for those angles at which the Livingston amplitude gets very small. The analogous plot for the Hanford to Livingston ratio is shown in Fig. 7.

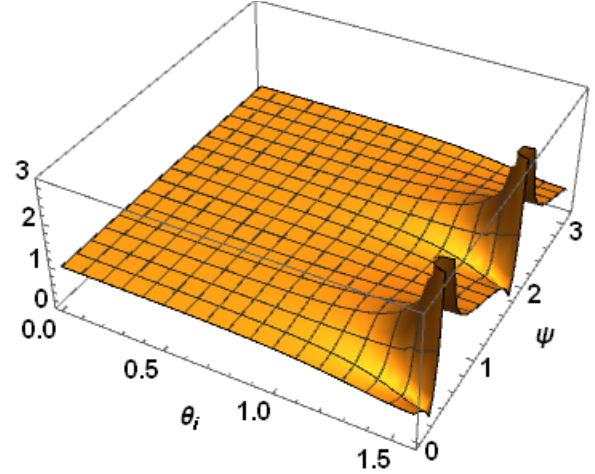


FIG. 7. The linear GR prediction of the ratio of the Hanford observatory strain signal amplitude to the Livingston amplitude as a function of the orbital angle of inclination θ_i and the polarization orientation angle ψ , both in radians.

We can see from Figs. 6 and 7 that the two ratios are approximately independent of the polarization orientation angle for $0 \leq \theta_i < 0.8$ rad. Under those conditions the observer is looking almost directly down on the orbital plane and, as mentioned before, in that case the two polarization modes have nearly equal amplitudes and the linear GR tensor polarization models predicts $H/L \approx 1$ and $V/L \approx 0.9$, both outside the range of observed ratios. That result indicates that if there is to be a match with the observed ratios, we need to look at larger values of θ_i and restricted ranges of the polarization orientation angle.

To compare the observed amplitude ratios quantitatively to those observed for GW170814, it is helpful to look at contour maps of the ratios as shown in the figures that follow. As mentioned previously, the ratios indicated by the observations can be estimated from the signals displayed in GW170814-Fig. 1. In what follows, we assume that the both the Hanford/Livingston amplitude ratio and the VIRGO/Livingston amplitude ratio fall in the range $[0.54 \leq (H/L \text{ or } V/L) \leq 0.82]$.

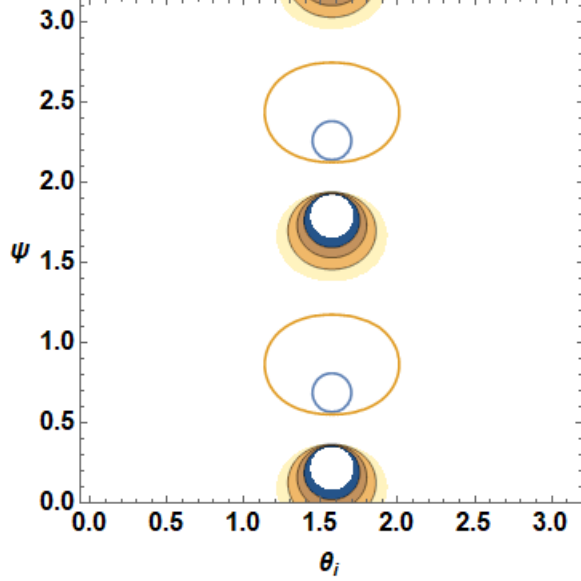


FIG. 8. A contour plot of the linear GR tensor polarization model calculation of the VIRGO/Livingston and Hanford/Livingston GW strain signal amplitude ratios that fall within the uncertainty range of the pre-merger observations, plotted as a function of θ_i and ψ , both in radians. Source location: 45° S, 73° W. Solid line contours bound the V/L ratio range. The shaded areas indicate the H/L ratio range.

Figure 8 shows the linear GR calculation of the range of angles of inclination and polarization orientation angles consistent with the observed H/L and V/L amplitude ratios during the pre-merger inspiral. The region between the solid curves indicates the range of θ_i and ψ that gives ratios consistent with the V/L amplitude observations (taking into account the range of uncertainty). The shaded regions indicate the range of θ_i and ψ and that give H/L amplitude ratios consistent with the observations (taking into account the range of uncertainty). Since the regions do not overlap, we conclude that the observations cannot be explained by the GR tensor polarization model with the given source location.

There are three options to explain the disagreement between the calculations and the observations:

- The calibration of the strain signal amplitudes at one or more of the observatories is incorrect.
- The polarization properties of the GWs are more complicated than those given by the standard GR tensor polarization model.

- The GW source location (or equivalently the GW wave propagation direction) is not correct.

We will explore the second and third possibilities below and assume that the amplitude ratios inferred from GW170814-Fig.1 are correct. But first, let's examine vector model predictions.

Vector polarization model

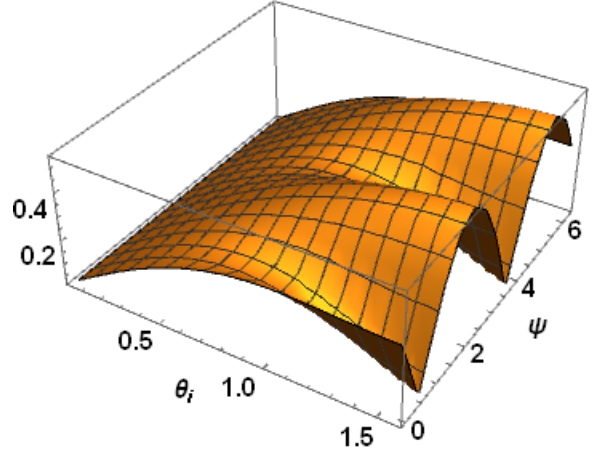


FIG. 9. The vector polarization model predictions for the Livingston GW strain signal amplitude (arbitrary units) as a function of the orbital angle of inclination θ_i and the polarization orientation angle ψ , both in radians.

Figure 9 shows a plot of the Livingston observatory GW strain signal amplitude as predicted by the vector polarization model. Note that for small values of the angle of inclination θ_i , the amplitude is approximately independent of the polarization orientation angle ψ : in this range the predicted GW emission is approximately circularly polarized, so there is no orientation angle dependence. Note also that the amplitude goes to zero as $\theta_i \rightarrow 0$. In the vector model there is no gravitational wave emission perpendicular to the plane of the orbit, in contrast to the GR tensor polarization model for which the power emission is maximum in that direction.

As $\theta_i \rightarrow \pi/2$, the vector polarization “x-mode” amplitude goes to zero, and the emission is almost completely linearly polarized. In that case, the amplitude is proportional to $|\sin \psi|$, repeating every π radians, characteristic of vector linear polarization (like E&M linear polarization). The plot for $\theta_i \rightarrow \theta_i + \pi/2$ is just the mirror image of the plot shown in Fig. 9. The Hanford and VIRGO

amplitudes are similar but with shifts in their ψ dependence.

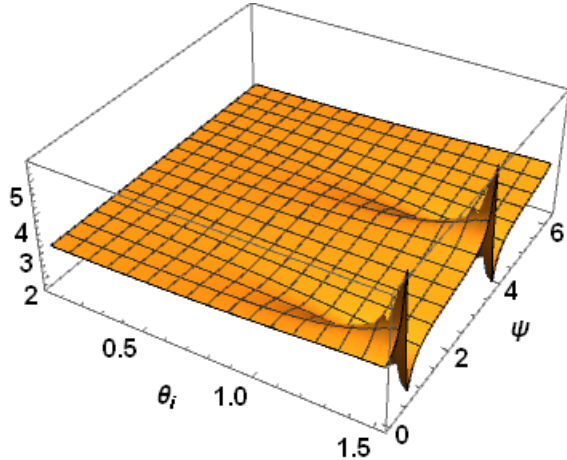


FIG. 10. The vector model predictions of the ratio of the VIRGO GW strain signal predictions of the ratio of the VIRGO GW strain signal to the Livingston amplitude as a function of the orbital angle of inclination θ_i and the polarization orientation angle ψ , both in radians.

Figure 10 shows the vector model prediction for the ratio of the VIRGO/Livingston amplitudes. Note that for most of the angular ranges, the ratio is about 3, much larger than the observed amplitude ratio of about 0.7 in the pre-merger inspiral for GW170814. However, there is a small range of angles near $\theta_i = \pi/2$ and $\psi \approx 0.7$ and 3.8 where the ratio is considerably smaller. The large spikes occur where the Livingston amplitude is very small.

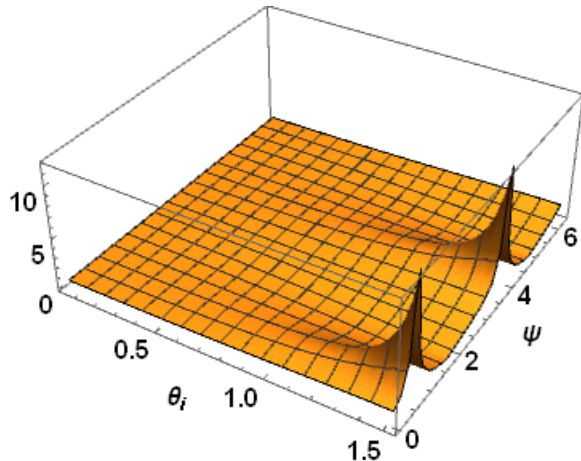


FIG. 11. The vector model prediction for the ratio of the Hanford GW strain signal amplitude to the Livingston amplitude as a function of the orbital angle of inclination θ_i and the polarization orientation angle ψ , both in radians.

Figure 11 shows the Hanford/Livingston amplitude ratio predicted by the vector polarization model. Over most of the angular range the ratio is about 1-2. The large spikes occur where the Livingston amplitude is very small.

Now let's use a contour plot to look at the amplitude ratios more quantitatively.

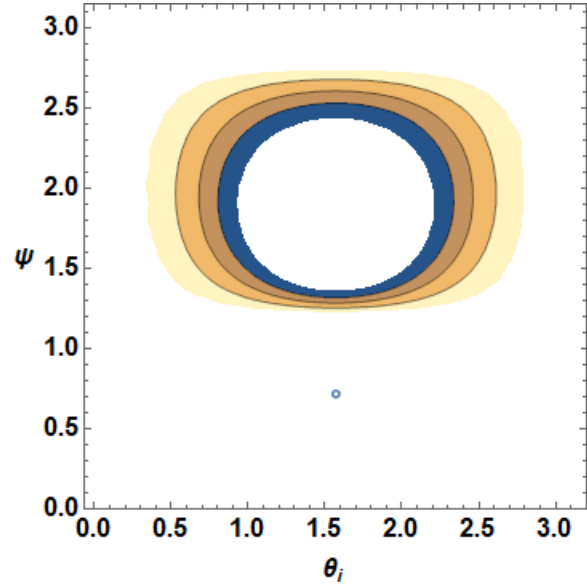


FIG. 12. A contour plot indicating the vector polarization model calculation of the VIRGO/Livingston and Hanford/Livingston GW strain signal amplitude ratios that fall within the range of the pre-merger inspiral observations (taking into account the uncertainty range) plotted as a function of θ_i and ψ , both in radians. Source location: -45° S, 73° W. Solid line contours indicate the V/L the range of θ_i and ψ that give amplitude ratios consistent with the observations. The shaded areas indicate the H/L ratio range.

We see from Fig. 12 that there is no overlap of the two regions associated with H/L ratios and the V/L ratios. Hence, we conclude that the vector model, like the tensor polarization model, cannot account for the observed pre-merger amplitude ratios for this GW source location.

VI. CHANGING THE GW SOURCE LOCATION

We now look at how the amplitude ratios vary if we change the GW source latitude and longitude. As noted previously, there is a substantial range of angles consistent with the uncertainties in the wavefront arrival times at the detectors. After exploring several angular values, we found that angles near $\theta_{lat} = -34^\circ$ and $\phi_{long} = 69^\circ$ W (shown as a filled circle in Fig. 4) give some overlap between the predictions of *both* the tensor polarization model and

the vector polarization model. For the tensor polarization model, we find the following contour plot:

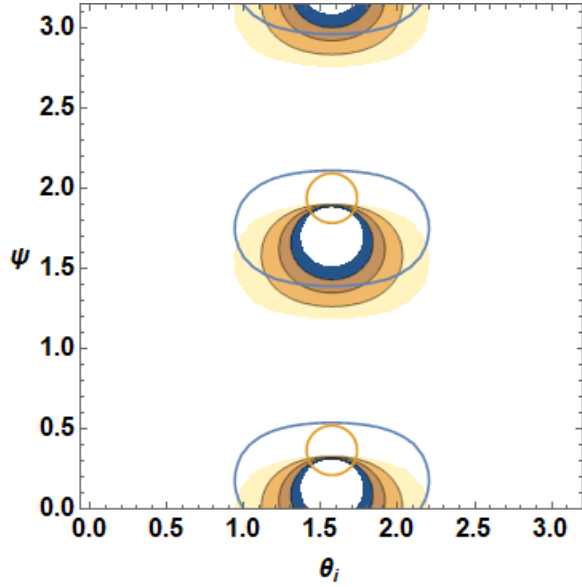


FIG. 13. A contour plot indicating the tensor polarization model calculations for the VIRGO/Livingston and Hanford/Livingston GW strain signal amplitude ratios that agree with the pre-merger observations (taking into account the range of uncertainty) plotted as a function of θ_i and ψ , both in radians. Source location: $-34^\circ, 69^\circ$ W. Solid line contours indicate the range of θ_i and ψ , that give V/L ratios consistent with the observations. The shaded areas indicate the H/L ratio range.

In Fig. 13, there are now overlap regions near $\theta_i \approx 1.35$ rad and $\psi \approx 0.2$ rad (with mirror regions with respect to the $\theta_i = \pi/2$ line) indicating that there is a small range of inclination and polarization orientation angles for which the tensor polarization model predictions agree with the observed pre-merger amplitude ratios. Note that the pattern repeats when $\psi \rightarrow \psi + \pi/2$.

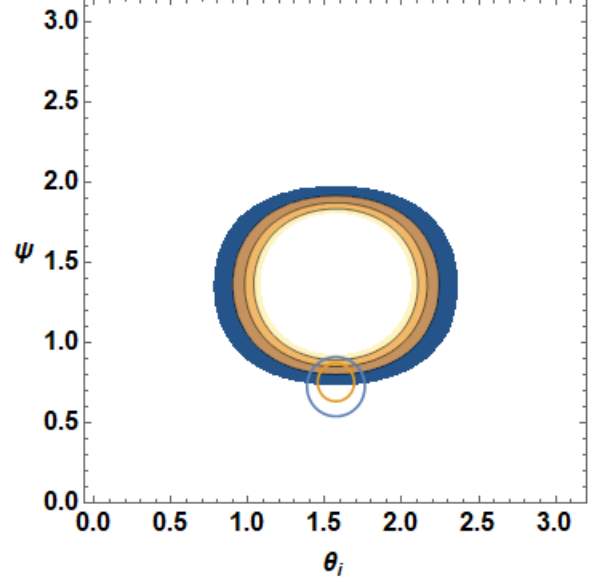


FIG. 14. A contour plot indicating the vector polarization model calculation of the VIRGO/Livingston and Hanford/Livingston GW strain signal amplitude ratios that fall within the uncertainty range of the pre-merger observations plotted as a function of θ_i and ψ , both in radians. Source location: $-34^\circ, 69^\circ$ W. Solid line contours indicate the V/L ratio range. The shaded areas indicate the H/L ratio range.

Figure 14 shows analogous results for the vector polarization model. Note that we now have overlap regions near $\theta_i \approx 1.45$ rad and $\psi \approx 0.8$ rad (with mirror regions with respect to the $\theta_i = \pi/2$ line). The pattern repeats for $\psi \rightarrow \psi + \pi$ (not shown).

We conclude that both the tensor polarization and, surprisingly, the vector polarization models can account for the observed pre-merger amplitude ratios for GW source locations just outside the LIGO-VIRGO 90% confidence limits, but only for a small range of θ_i and ψ . In other words, the observed amplitude ratios provide detailed information about the range of θ_i and ψ consistent with the observations.

More importantly, we see that the pre-merger inspiral observations do not rule out vector contributions to the GW polarization. Based on a detailed analysis of an E&M-like model (Hilborn, 2018), we anticipate that any vector model contribution to the GW amplitude will be about 1/4 the contribution from the linear GR tensor model for a given set of binary masses.

Although these results might lead one to claim that GR's account of GWs is incomplete, we argue more conservatively that the observed GW signal amplitudes, which are difficult to measure precisely due to noise in the signals, particularly during the

pre-merger inspiral, should be carefully re-examined before we can draw definitive conclusions about the vector polarization contributions.

VII. PHASE DIFFERENCES

As mentioned previously, the observed amplitude ratios are intimately tied to the GW source sky location and the polarization orientation as shown in the previous section. The signals also depend on phase differences of the GW signals at the observatories due to the orientations of the detectors' arms relative to the GW polarization orientation. Let us now look at the tensor polarization predictions for the phase differences between the VIRGO and Livingston signals and the Hanford and Livingston signals, ignoring for the moment the travel time delays between the observatories.

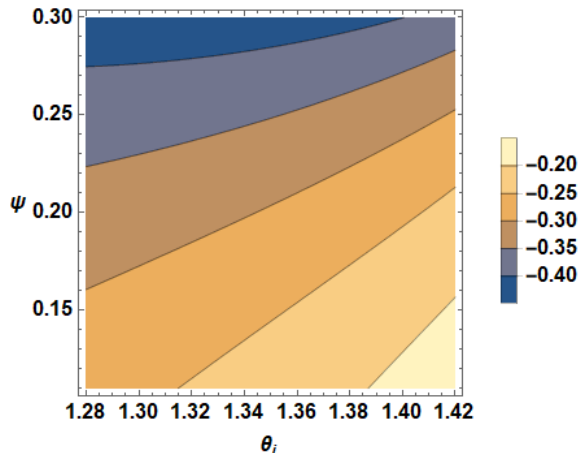


FIG. 15. A contour plot of the tensor model calculation of the VIRGO-Livingston phase difference predictions (in radians) as a function of the orbital angle of inclination θ_i and the polarization orientation angle ψ (both in radians) for the region in Fig. 13 where the predictions overlap the observed amplitude ratios. Source location: $-34^\circ, 69^\circ$ W.

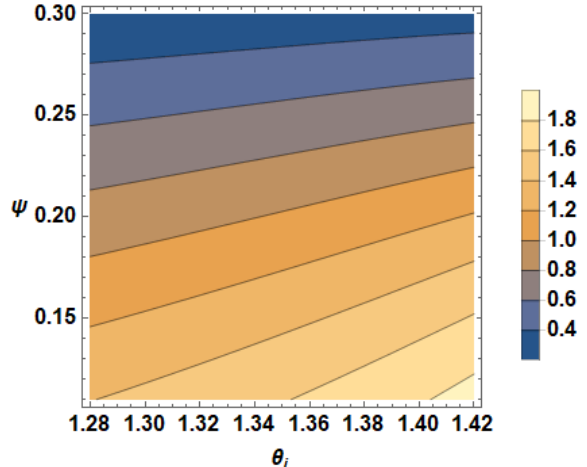


FIG. 16. A contour plot of the Hanford-Livingston tensor model phase difference predictions (in radians) as a function of the orbital angle of inclination θ_i and the polarization orientation angle ψ (both in radians) for the region in Fig. 13 where the predictions overlap the observed amplitude ratios). Source location: $-34^\circ, 69^\circ$ W.

Figures 15 and 16 indicate that the tensor model phase differences between VIRGO and Livingston are only a few tenths of a radian. In the convention used here (see Eq. (5)), a negative phase difference implies an additional time delay between Hanford and Livingston beyond the time-of-flight delay. For Hanford and Livingston, the tensor model phase shift is about -1.2 rad. For a gravitational wave frequency of about 60 Hz (see GW170814-Fig. 1), a VIRGO-Livingston -0.3 radian phase shift corresponds to a time delay of about 0.8 ms, well within the range of uncertainty in the relative timing measurements, while the Hanford-Livingston -1.2 rad phase shift is equivalent to a time delay of about 3 ms.

Careful examination of GW170814-Fig. 1 shows the observed time delay for the Hanford signal relative to the Livingston signal is about 12 ms in the pre-merger regime. Subtracting the 3 ms phase offset, gives a travel time delay of about 9 ms, in rough agreement with the cited 8 ms arrival time delay. (The 8 ms delay is the GW170814-Fig. 1 observed arrival time difference for Hanford relative to Livingston for the sharp features in the *merger* phase of the signal.) Similarly, the observed pre-merger time delay for VIRGO relative to Livingston is about 14 ms, consistent with a small phase shift and the 14 ms travel time between Livingston and VIRGO.

VIII. DISCUSSION

In this paper, we have demonstrated that there is an inconsistency among the reported¹ GW170814 source location, the ratios of the observed pre-merger

amplitudes (GW170814-Fig. 1) for the Livingston, Hanford, and VIRGO observatories and predictions of the GW polarization properties. That inconsistency is manifest in examining the orbital inclination angle and polarization orientation angle dependence of the GW amplitude ratios among the three sites. The inconsistency shows up in both the standard linear GR tensor polarization predictions and the predictions of vector polarization models.

We also found that source locations just outside the 90% confidence range of the GW170814 locations do give tensor polarization amplitude and phase shift predictions consistent with the observed amplitude ratios. Unexpectedly, we find that vector polarization models also give predictions consistent with observations in that same range. We emphasize, however, that there is a need to re-examine carefully the observed amplitude ratios before concluding that GWs might have a vector polarization contribution.

Acknowledgements

The author thanks Nicolas Arnaud of the EGO/Virgo Outreach Team for directions to the gravitational wave detector location and orientation information. Carver Mead (CalTech) and Thomas A. Moore (Pomona College) provided several helpful discussions and comments.

This research has made use of data, software and/or web tools obtained from the LIGO Open Science Center (<https://losc.ligo.org>), a service of LIGO Laboratory, the LIGO Scientific Collaboration and the Virgo Collaboration. LIGO is funded by the U.S. National Science Foundation. Virgo is funded by the French Centre National de Recherche Scientifique (CNRS), the Italian Istituto Nazionale della Fisica Nucleare (INFN) and the Dutch Nikhef, with contributions by Polish and Hungarian institutes.

References

1. Abbott, B. P. et al, “GW170814: A Three-Detector Observation of Gravitational Waves from a Binary Black Hole Coalescence,” *Phys. Rev. Lett.* **119**, 141101-1-16 (2017).
2. Thomas Callister, Sylvia Biscoveanu, Nelson Christensen, Maximiliano Isi, Andrew Matas, Olivier Minazzoli, Tania Regimbau, Mairi Sakellariadou, Jay Tasson and Eric Thrane, “Polarization-Based Tests of Gravity with the Stochastic Gravitational-Wave Background,” *Phys. Rev. X* **7**, 041058-1-27 (2017).
3. Anatoly A. Svidzinsky, “Comment on “Probing gravitational wave polarizations with signals from compact binary coalescences”,” arXiv:1712.07181v1 [gr-qc] 1-4 (2017).
4. Maximiliano Isi, Matthew Pitkin and Alan J. Weinstein, “Probing dynamical gravity with the polarization of continuous gravitational waves,” *Phys. Rev. D* **96**, 042001-1-27 (2017).
5. Douglas M. Eardley, David L. Lee, Alan P. Lightman, Robert V. Wagoner and Clifford M. Will, “Gravitational-Wave Observations as a Tool for Testing Relativistic Gravity,” *Phys. Rev. Lett.* **30**, 884-886 (1973).
6. Douglas M. Eardley, David L. Lee and Alan P. Lightman, “Gravitational-Wave Observations as a Tool for Testing Relativistic Gravity,” *Phys. Rev. D* **8**, 3308-3321 (1973).
7. Clifford M. Will, “The Confrontation between General Relativity and Experiment,” arXiv: 1403.7377, (2014).
8. Anatoly A. Svidzinsky, “Vector theory of gravity: Universe without black holes and solution of the dark energy problem,” *Phys. Scr.* **92**, 125001-1-54 (2017).
9. Carver Mead, “Gravitational Waves in G4v,” e-print arXiv:gr-qc/1503.04866v1 (2015).
10. Robert C. Hilborn, “Gravitational waves without general relativity,” *Am. J. Phys.* **86**, (March, 2018).
11. Stephen Fairhurst, “Localization of transient gravitational wave sources: beyond triangulation,” arXiv: 1712.04724v1 [gr-qc] 1-27 (2017).
12. C. Misner, K. Thorne and J. A. Wheeler, *Gravitation* (W. H. Freeman, New York, 1973).
13. Thomas A. Moore, *A General Relativity Workbook* (University Science Books, Mill Valley, California, 2013).
14. Maximiliano Isi, Alan J. Weinstein, Carver Mead and Matthew Pitkin, “Detecting Beyond-Einstein Polarizations of Continuous Gravitational Waves,” *Phys. Rev. D* **91**, 082002-1-19 (2015).
15. Maximiliano Isi and Alan J. Weinstein, “Probing gravitational wave polarizations with signals from compact binary coalescences,” LIGO-P1700276 arXiv: 1710.03794v1 [gr-qc] (2017).
16. Liudmila Fesik, “Polarization states of gravitational waves detected by LIGO-Virgo antennas,” arXiv:1706.09505v1 [gr-qc] 1-49 (2017).
17. Bruce Allen, “Can a “pure vector” gravitational wave mimic a “pure tensor” one?” arXiv1801.04800v1 1-8 (2018). The Appendix of this paper gives details of the LIGO-VIRGO detectors' unit vectors in terms of the Earth-fixed coordinate system.
18. LIGO-VIRGO Collaboration, *LIGO Interferometric Detector Constants*, <https://losc.ligo.org/s/param/position.txt>, 2016).
19. LIGO-VIRGO Collaboration, *GW170814 Fact Sheet*, <https://losc.ligo.org/events/GW170814/>, 2017).
20. Richard H. Price and Gaurav Khanna, “Arrival Times of Gravitational Radiation Peaks for Binary Inspiral,” arXiv: 1607.04226v2 [gr-qc] 1-12 (2016).
21. Luc Blanchet, Bala R. Iyer, Clifford M. Will and Alan G. Wiseman, “Gravitational waveforms from inspiralling compact binaries to second-post-Newtonian order,” *Class. Quantum Grav.* **13**, 575-584 (1996).
22. Lawrence E. Kidder, “Coalescing binary systems of compact objects to (post)^{5/2}-Newtonian order. V. Spin effects,” *Phys. Rev. D* **52**, 821-847 (1995).